Journal of
Materials Chemistry C

ROYAL SOCIETY
OF CHEMISTRY

PAPER

View Article Online
View Journal | View Issue

Check for updates

Cite this: *J. Mater. Chem. C*, 2024, **12**, 533

Band-bowing effects in lead-free double $Cs_2AgBi_xSb_{1-x}Cl_6$ perovskites and their anion-exchanged derivatives†

Oleksandr Stroyuk, *[a] Oleksandra Raievska,[a] Anastasia Barabash,[b]
Riley W. Hooper,[c] Vladimir K. Michaelis,[c] Jens Hauch[ab] and
Christoph J. Brabec[ab]

Received 2nd November 2023,
Accepted 4th December 2023

DOI: 10.1039/d3tc04004f

rsc.li/materials-c

Green synthesis of lead-free $Cs_2AgBi_xSb_{1-x}Cl_6$ solid-solution double perovskites and their conversion into bromide and iodide derivatives is reported. Interaction of the single-phase $Cs_2AgBi_xSb_{1-x}Cl_6$ double perovskites with sodium iodide in 2-propanol/glycerol yields $Cs_3Bi_{2x}Sb_{2(1-x)}I_9$ derivatives with varied Bi/Sb ratio, while the similar anion exchange with sodium bromide results in mixtures of $Cs_3Bi_{2x}Sb_{2(1-x)}Cl_3Br_6$ and $Cs_2AgBi_xSb_{1-x}Cl_2Br_4$. A band-bowing effect is revealed for the starting chloride perovskites and the anion-exchange products, with the indirect band gap of intermediate Bi/Sb mixed compounds being significantly lower than the band gaps of corresponding Bi- and Sb-pure products. Solid-state nuclear magnetic resonance spectroscopy uncovered that the band-bowing originates from the lattice disorder of mixed Bi/Sb halide compounds, thus highlighting a new approach for the bandgap design of halide perovskites.

Introduction

Lead-free halide materials attract considerable attention as a potential alternative for lead-based hybrid perovskites, the latter excelling as a new class of highly efficient and variable absorbers for thin-film photovoltaics (PV).[1–5] The substitution of Pb^{2+} with various bi-valent cations as well as the introduction of M^+/M^{3+} combinations instead of Pb^{2+}/Pb^{2+} pairs, yields lead-free perovskites with a broad compositional variability, unrivalled by their Pb-based ancestors. The efficiency of PV devices incorporating lead-free perovskites is, though, still comparatively low,[1–5] mostly due to larger band gaps and inferior charge carrier mobility, showing room for further progress in the functional design of such PV materials.

The field of double lead-free $A^I_2M^IM^{III}X_6$ perovskites, where A^I is an alkali cation and X is a halide, is dominated by bismuth(III) compounds where Bi^{3+} is typically combined with Ag^+ or Na^+, and $A^I = Cs^+$, for example, $Cs_2NaBiCl_6$ or $Cs_2AgBiBr_6$.[1–8] The double perovskite structure is very labile allowing multiple substitutions to be realized simultaneously on M^I, M^{III}, and X sites. In this way, Bi^{3+} is typically alloyed with In^{3+} or Sb^{3+} on the M^{III} sites, while the M^I sites are filled with mixtures of Ag^+ and Na^+.[1–8] Recently, many new Bi-halide compounds have been synthesized and tested as PV materials, such as $CsBi_3I_{10}$ or Cu_2AgBiI_6, combined into the class of ‘‘perovskite-inspired materials’’ and revealing a broad compositional and structural versatility and promises for indoor photovoltaics.[1,4,9,10]

Similar to the Pb-based halide perovskites, the lead-free Bi-based compounds show a strong dependence of the light sensitivity range on the nature of halide X, with band gaps of bromide compounds approaching 2 eV and those of iodide compounds – coming below this imaginary threshold and approaching values typical for Pb perovskites.[2,6,7] At the same time, the synthesis of Bi-based double bromide and iodide perovskites is typically challenging, as it requires a large thermal input, an inert atmosphere, and reactive, toxic, or volatile

---

[a] *Forschungszentrum Jülich GmbH, Helmholtz-Institut Erlangen Nürnberg für Erneuerbare Energien (HI ERN), 91058 Erlangen, Germany. E-mail: o.stroyuk@fz-juelich.de*
[b] *Friedrich-Alexander-Universität Erlangen-Nürnberg, Materials for Electronics and Energy Technology (i-MEET), Martensstrasse 7, 91058 Erlangen, Germany*
[c] *Department of Chemistry, University of Alberta, 11227 Saskatchewan Drive, Edmonton, Alberta, T6G 2G2, Canada*

† Electronic supplementary information (ESI) available: Elemental composition of chloride, bromo-chloride, and iodide compounds; examples of XRD patterns of CABSC perovskites and products of partial chlorine-to-bromine substitution; relationships between nominal and actual element fractions; a collection of SEM images and EDX spectra of chloride, bromide, and iodide compounds with different Bi/Sb ratio; examples of absorption spectra of chloride, bromide, and iodide compounds plotted in Tauc coordinates for direct and indirect transitions; ^{209}Bi MAS NMR spectra for chloride and iodide compounds; relationships between NMR spectral features and composition of Br-substituted CABSC compounds; examples of Raman spectra of bromide compounds. See DOI: **https://doi.org/10.1039/d3tc04004f**

precursors (such as HBr or HI) as well as due to the inherent thermal and/or redox instability of many final perovskites.[6,7]

The broadly explored chemistry of lead perovskites indicates that this problem can be addressed by an indirect synthesis of bromide or iodide compounds from corresponding chlorides *via* anion exchange reactions.[6,7] The feasibility of this approach for a controlled transformation of lead-free double perovskites was shown by Gamelin *et al.* who reported the anion-exchange-driven conversion of nanocrystalline $Cs_2AgBiCl_6$ into $Cs_2AgBiBr_6$ and further – into Cs_2AgBiI_6 by using trimethylsilyl halides as exchange agents.[11] This pioneering report showed the potential and flexibility of anion-exchange reactions in the chemistry of lead-free halide perovskites.[6,7] Simultaneously, it outlined the challenges, particularly the need for more stable and sustainable anion exchange agents that can be used at lower temperatures and in polar solvents required by green chemistry.

In the present paper, we report the structural and spectral properties of bromide- and iodide-containing materials produced *via* anion exchange from $Cs_2AgBi_xSb_{1-x}Cl_6$ (CABSC) perovskites with a varied Bi/Sb ratio. The key point of our report is that the anion exchange is performed in very mild conditions, including room temperature, an open-air atmosphere, and the application of NaBr and NaI as readily available, stable, and non-volatile bromide and iodide precursors. At that, the original microcrystalline CABSC double perovskites are synthesized by using a "green" protocol based on the recently introduced mild synthesis of $Cs_2Ag_xNa_{1-x}Bi_yIn_{1-y}Cl_6$ perovskites.[12,13]

The paper focuses on the spectral characteristics of $Cs_2AgBi_xSb_{1-x}Cl_6$ perovskites and their anion-exchanged derivatives probed by absorption, Raman, and solid-state nuclear magnetic resonance (NMR) spectroscopies. We discuss optical band-bowing observed both for the original perovskites and for the products of chloride-to-bromide and chloride-to-iodide exchange as well as spectral evidence of the local lattice disorder as one of the reasons for the band-bowing behavior.

Materials and methods

Synthesis of $Cs_2AgBi_xSb_{1-x}Cl_6$ microcrystals

Two precursors were prepared, separately containing M^{III} and M^I compounds. The first precursor was prepared by adding 200 μL of 12.0 M aqueous HCl solution and 500 μL of 2-propanol to 100 μL of 1.0 M aqueous $SbCl_3$ ($BiCl_3$, $SbCl_3 + BiCl_3$) solution, the latter containing 4.0 M HCl to avoid hydrolysis of M^{III} salts. The second precursor solution was prepared by adding 100 μL of 1.0 M aqueous $AgNO_3$ solution to 100 μL of deionized (DI) water followed by 25 μL of aqueous 25% ammonia solution, 500 μL of 2-propanol, and 60 μL of aqueous 4.0 M solution of Cs acetate (CsAc). All additions were performed under vigorous stirring. An excess of CsAc (20%) was introduced to shift the equilibrium toward the deposition of the perovskite phase from the water/2-propanol mixture. The synthesis of microcrystalline CABSC is performed at ambient temperature in an open-air environment.

The presence of excessive CsAc enhances the precipitation and suppresses the formation of $Cs_3(Sb,Bi)_2Cl_9$ compounds with a lower $Cs^I:M^{III}$ ratio (1.5 : 1.0), routing the reaction to the target $Cs_2Ag(Sb,Bi)Cl_6$ double perovskites (2.0 : 1.0). We note that the stock solutions with concentrations above 1.0 M should be prepared by dissolving the required amount of the salt in a minimal volume of water and adding then DI water to reach the total calculated volume of solution.

The second precursor solution is then rapidly added to the first precursor solution at intense stirring for a minimum of 5 min. Afterward, the resulting suspension is kept in a closed vial without stirring overnight (for at least 12–14 h) to reach complete crystallization. After ripening for 12–14 h the supernatant solution is eliminated from the precipitate, 1 mL of 2-propanol is added to the precipitate, and the resulting suspension is centrifuged at 2000 rpm for 2 min. The supernatant is discarded again, 1.0 mL of 2-propanol is added, and the centrifugation is repeated to purify the product from residual salts. The final samples are dried and stored in the dark at room temperature. The above-described synthetic procedure yields *ca.* 50 mg of each product.

The samples for structural characterization and optical measurements are produced from freshly prepared and purified precipitates by adding 200 μL 2-propanol and drop-casting 30 μL of the final suspension into a 1 cm^2 glass substrate.

Anion exchange

CABSC perovskites with varied Bi/Sb ratios were reacted with NaBr and NaI dissolved in 2-propanol/glycerol mixtures at room temperature and in an open-air environment. The 2-propanol/glycerol mixtures were prepared by mixing 50 g of glycerol with 100 mL of 2-propanol. In a typical procedure, 1.4 mL of 2-propanol/glycerol mixture was mixed with *ca.* 0.05 g of freshly prepared and purified chloride double perovskite, and then 0.2 mL of aqueous 4.0 M NaBr (NaI) solution was added under vigorous stirring. The stirring was continued for 30 min, and the precipitate was separated from the supernatant containing dissolved NaCl by centrifugation at 2000 rpm for 2 min. Then, 1 mL of 2-propanol was added, and centrifugation was repeated. In a series with varied NaBr concentrations, the total volume of water in the mixture was kept constant. The presence of glycerol is necessary to dissolve NaCl released during the anion exchange, which has a low solubility in 2-propanol.

X-Ray diffraction (XRD) patterns were registered using a Panalytical X'pert powder diffractometer with filtered Cu K_α radiation (λ = 1.54178 Å) and an X'Celerator solid-state stripe detector in the Bragg–Brentano geometry in an angle range of 2θ = 5–100° with a step rate of 0.05° per min. The XRD patterns were subjected to a Rietveld refinement procedure using MAUD software. Scanning electron microscopy (SEM) imaging and energy-dispersive X-ray spectroscopic (EDX) analysis were performed using a JEOL JSM-7610F Schottky field emission scanning electron microscope operating under 15–20 kV acceleration voltage equipped with an X-Max 80 mm^2 silicon drift detector (Oxford Instruments).

Reflectance spectra were recorded using a BlackComet spectrometer (StellarNet Inc.) and a 75 W Xenon lamp (Thorlabs) as an excitation source. The spectra were registered with an optical Y-fiber probe in identical geometry for samples and a scattering reference (ultra-pure $BaSO_4$, Alfa-Aesar). The reflectance spectra were transformed into absorption spectra using the Kubelka–Munk formula and the reference.

Raman spectra were registered on a WITec alpha700 confocal Raman microscope equipped with a UHTS 300 spectrometer and a 532 nm laser.

Solid-state nuclear magnetic resonance (NMR) spectroscopy was performed on either a Bruker AVANCE III HD 400 (B_0 = 9.39 T) or Bruker Avance NEO 500 (B_0 = 11.75 T) NMR spectrometer equipped with a 4 mm double-resonance (H/X) Bruker magic-angle spinning (MAS) probe. The ^{133}Cs MAS NMR spectra were acquired using a Bloch-decay experiment with a 4.0 μs $\pi/2$ pulse (ν_{rf} = 62.5 kHz), 4 co-added transients, a recycle delay of 300 s, and a spinning frequency of 14 kHz. ^{133}Cs NMR spectra were referenced to a secondary standard (solid CsCl to 223.2 ppm) with respect to 0.5 M CsCl ($\delta(^{133}Cs)$ = 0.00 ppm). ^{209}Bi NMR (MAS; ν_{rot} = 14 kHz, and non-spinning) spectra were acquired using a Hahn echo experiment with a 1.0 μs $\pi/2$ pulse (ν_{rf} = 250 kHz), 32 000 co-added transients, and recycle delay of 0.1 s. NMR spectra were referenced with respect to saturated $Bi(NO_3)_3$ in HNO_3 ($\delta(^{209}Bi)$ = 0.00 ppm). All NMR spectra were processed with Bruker TopSpin 3.6.2.

Results and discussion

Chloride-based compounds

X-ray diffraction patterns of $Cs_2AgBi_xSb_{1-x}Cl_6$ (CABSC) double perovskites show a set of reflections characteristic for a cubic *Fm*3*m* space group[14–19] in the entire range of Bi-to-Sb ratios (Fig. 1a). Rietveld refinement of the XRD patterns (see examples in ESI,† Fig. S1) shows that CABSC double perovskites are present as a single phase with no detectable phase admixtures.

EDX analysis of CABSC compounds revealed that the actual Bi fraction in final products (x_a) follows very closely the nominal Bi fraction (x) set during the synthesis in the precursor solutions (ESI,† Table S1). The relationship between x_a and x is linear with the slope very close to unity (ESI,† Fig. S2a). The Cs/(Bi + Sb) and Ag/(Bi + Sb) ratios are close respectively to 2 and 1, following the expected stoichiometry, while the Cl/(Bi + Sb) ratio is typically around 5–5.5, indicating a certain deficiency of chloride anions in the perovskite structure (ESI,† Fig. S3 and Table S1).

The lattice parameter of CABSCs increases linearly with the actual Bi fraction x_a (Fig. 1b) showing the double perovskites to be ideal solid solutions obeying Vegard's law.[18,20] The lattice parameters of individual $Cs_2AgSbCl_6$ (L = 10.713 Å) and $Cs_2AgBiCl_6$ (L = 10.788 Å) are close to typically reported values.[14–19] The lattice expansion observed for Bi-containing compounds is caused by a larger cation size of Bi^{3+} (117 pm) as compared to Sb^{3+} (90 pm).[18]

Scanning electron microscopy of CABSC samples revealed randomly aggregated microcrystals with a broad distribution of grain sizes from *ca.* 0.5 to 5 μm (ESI,† Fig. S4, left column of images). No significant changes in the morphology were detected as x was elevated from 0 to 1.

Raman spectra of CABSC compounds are typical for double perovskites with prominent A_{1g}, E_g, and T_{2g} vibrational bands[16,17,19] observed for $Cs_2AgSbCl_6$ at 288 cm^{-1}, 215 cm^{-1}, and 121 cm^{-1}, respectively (Fig. 1c). As antimony is gradually substituted with bismuth the positions of phonon peaks shift

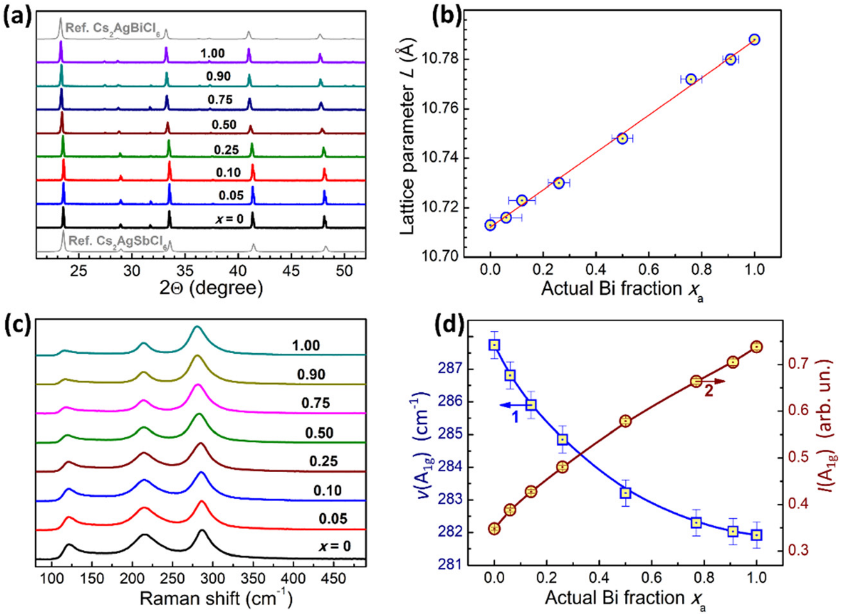

Fig. 1 (a) and (c) X-ray diffraction patterns (a) and Raman spectra (c) of $Cs_2AgBi_xSb_{1-x}Cl_6$ perovskites with varied nominal Bi fraction x. (b) and (d) Lattice parameter L (b), A_{1g} peak frequency $\nu(A_{1g})$ (d, scatter1), and the relative intensity of A_{1g} band $I(A_{1g})$ (d, scatter 2) of CABSC perovskites as a function of x_a; solid line in (b) represents the linear fit $L = 10.712 + 0.076x_a$ (coefficient of determination R^2 = 0.997); solid lines in (d) represent polynomial fits $\nu(A_{1g}) = 287.6 - 11.9x_a + 6.4x_a^2$ (R^2 = 0.996) and $I(A_{1g}) = 0.355 + 0.513x_a - 0.136x_a^2$ (R^2 = 0.999).

to lower frequencies, reaching 282 cm^{-1}, 212 cm^{-1}, and 115 cm^{-1}, respectively, for $Cs_2AgBiCl_6$. Both sets of frequencies are in accordance with previous reports.[16,17,19] The Raman data are consistent with the above conclusions about the single-phase and solid-solution character of CABSC double perovskites made from the powder XRD data.

The peak positions and relative intensities of the A_{1g} phonon band can be used for the spectral identification of the perovskite composition. Both the position (Fig. 1d, scatter 1) and relative intensity (Fig. 1d, scatter 2) show polynomial dependences on x_a, allowing Raman spectroscopy to be used as an express analytical tool for evaluating the bismuth content in CABSC double perovskites. The continuous changes of phonon frequencies of mixed double perovskites typically indicate homogeneous alloying, while the segregation of components results in discontinuous frequency variations.[19] The shift of the A_{1g} band peak from 288 cm^{-1} for CASC to 282 cm^{-1} for CABC is related to the increase in the metal(III)–chloride bond length, from 2.35 Å for Sb–Cl[16] to 2.70 Å for Bi–Cl.[20]

The absorption spectrum of antimony-pure (CASC) double perovskite shows a continuous band with an extended low-energy edge at *ca.* 2.8–3.0 eV (Fig. 2a, curve 1). The absorption edge of bismuth-pure (CABC) double perovskite is shifted to lower energy as compared to CASC and reveals an additional high-energy peak at *ca.* 3.5 eV (Fig. 2a, curve 4). Surprisingly, the intermediate mixed CABSC compounds showed a shift of the absorption edge to lower energies (see exemplary curves 2 and 3 in Fig. 2a), as compared to both pure compounds. This shift is evidenced by a much deeper yellow coloration of mixed compounds as compared to Sb- and Bi-pure phases (photographs in the insert in Fig. 2a).

By theory and experimental observations, CASC and CABC double perovskites were reported as indirect-band gap semiconductors.[15–17,19,21–23] The absorption spectra of these compounds show extended linear sections of the absorption edge when plotted in the coordinates of the Tauc equation both for indirect and direct allowed interband transitions (see examples in ESI,† Fig. S5). At that, the presentation of the spectra in the Tauc coordinates for indirect transitions gives a higher correspondence with the original spectrum, as compared with the direct-transition Tauc presentation. For this reason, as well as in agreement with previous reports, the indirect bandgaps were calculated and discussed in the present work for the CABSC series.

The indirect bandgap decreases as Sb is substituted with Bi from E_g = 2.82 eV for Sb-pure compound to 2.59 eV for CABSC with x_a = 0.26 (Fig. 2b). At higher Bi contents, the bandgap starts to increase reaching 2.77 eV for Bi-pure CABC perovskite.

Considering the single-phase character of CABSC double perovskites, this behavior can be attributed to the band-bowing effect, often observed for solid-solution semiconductors[24,25] including mixed-metal halide perovskite and perovskite-like compounds.[26–30] The band-bowing in perovskites was attributed to local inhomogeneities in the composition and lattice of the alloyed semiconductor compounds.[26,27] Alternatively, the non-linear bandgap behavior was related to an energy mismatch between atomic orbitals of two different metal cations contributing to the band edges.[28,31] For example, the band-bowing effects observed for alloyed $Cs_2AgBi_xSb_{1-x}Br_6$ (CABSB) perovskites were interpreted as a result of a mixing of Bi- and Sb-related electronic states.[31] Calculations based on the relativistic density functional theory (DFT) showed the conduction band minimum of CABSB to be dominated by Bi–Br interactions, and the valence band maximum – by Sb–Ag–Br interactions, resulting in the alloys having lower bandgaps as compared to CABB and CASB. At that, the bandgap reduction upon alloying was predicted even for CABSB alloys with uniform atomic distribution.[31] The DFT calculations of the compositional bandgap dependence of $Cs_2AgBi_xSb_{1-x}Cl_6$ perovskites showed indications of the band-bowing when spin–orbit coupling effects were taken into consideration.[32]

Similar band-bowing effects originating from the non-linear orbital mixing at the band edges on the bandgap of Bi/Sb-based halide alloys were reported for solution-precipitated microcrystalline $Cs_3(Bi_xSb_{1-x})_2Br_9$ double salts.[29] For these compounds, the minimal bandgap was found at Bi : Sb ratio close to 1 : 1 both experimentally and by DFT calculations.[29] For the same phase-pure $Cs_3(Bi_xSb_{1-x})_2Br_9$ alloys, but produced *via* a

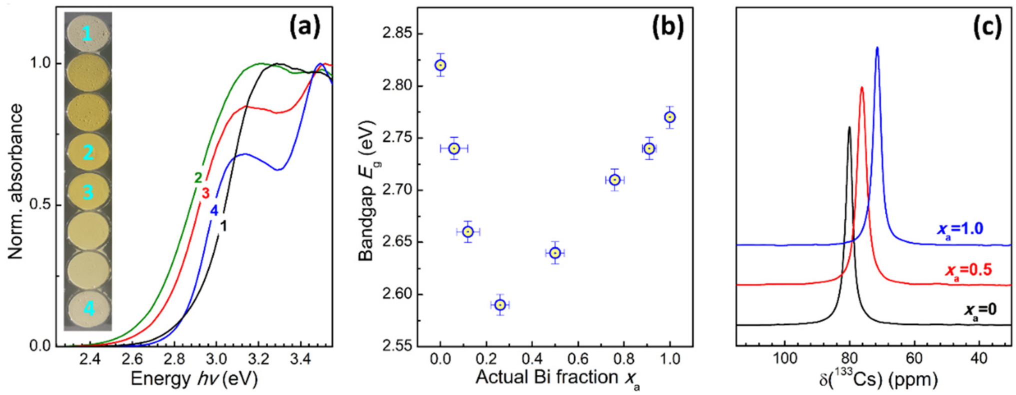

Fig. 2 (a) Normalized absorption spectra of CABSC double perovskites with varied nominal Bi fraction x = 0 (curve 1), 0.25 (2), 0.50 (3), and 1.00 (4), insert: photographs of CABSC double perovskites with a varied x (numbers correspond to absorption spectra). (b) Indirect bandgap E_g of CABSC double perovskites as a function of the actual Bi fraction x_a. (c) ^{133}Cs MAS NMR spectra of CABSC double perovskites with different x_a (ν_{rot} = 14 kHz; B_0 = 9.4 T).

mechano-chemical treatment of mixtures of $Cs_3Bi_2Br_9$ and $Cs_3Sb_2Br_9$, the lowest bandgap was observed at $x = 0.2–0.3$.[30] The ambiguity in the reported position of the lowest bandgap[29,30] can indicate that a combination of different reasons is responsible for the observed band-bowing effects. These reasons can be both of a chemical nature as assumed in ref. 28 and 31 but also can stem from local lattice disorder and local strain effects, related to the presence and inhomogeneous mixing of two different M^{III} cations. For double halide perovskites, such disorder-induced bandgap narrowing was reported for $Cs_2AgBiBr_6$, originating from Ag–Bi disorder.[33] Theoretical modeling of this compound showed the bandgap decreasing from 1.93 eV for a totally ordered lattice to 0.44 eV for randomly distributed cations.[34] The strain was reported to alter dramatically the lattice and electronic structure of Sb-pure CASC perovskite. For example, highly strained CASC single crystals[17] showed a lattice parameter and bandgap of 10.388 Å and 1.82 eV, respectively, which increased to 10.713 Å and 2.55 eV after the strain release by grinding with no detectable changes in the chemical composition between the original single crystal and ground polycrystalline CASC powder.[17]

The assumption of random Sb/Bi substitution made from powder XRD and Raman data is also supported by the ^{133}Cs MAS NMR spectroscopy of selected CABSC double perovskites. Each Cs cation is surrounded by 12 halide anions making it an ideal indicator that responds to any changes in the symmetry or composition of the perovskite lattice.[35–37]

The CABSC double perovskites reveal a single Cs-related peak (Fig. 2c) following the expected lattice symmetry. This observation supports the conclusion on the solid-solution character of pure crystalline materials, with trace quantities (<1%) of residual CsCl salt (δ_{iso} = 223 ppm).[35–37] The isotropic chemical shift (δ_{iso}) is observed at 80 ppm for CASC (x_a = 0), lowering to 76 ppm for the mixed CABSC compound with x_a = 0.50 and further, to 72 ppm, for CABC double perovskite (x_a = 1.00).

The monotonous shift of the ^{133}Cs peak indicates the formation of solid-solution $Cs_2AgBi_{0.5}Sb_{0.5}Cl_6$ compound, complimenting the XRD and Raman data, above. At the same time, the spectral width of the peaks increases, from 2.6 ppm for CASC to 3.3 ppm for CABSC, then decreasing again to 2.7 ppm for CABC perovskite. Analysis of the first-order quadrupolar interaction confirms a negligible second-order quadrupolar contribution to the central transition. Hence, the broadened ^{133}Cs resonance of the mixed CABSC can be related to a greater medium-range lattice disorder of this compound due to Sb/Bi mixing in the second coordination sphere as compared to antimony- and bismuth-pure lattices.[36,37]

Further analysis reveals a single spinning sideband pair which is due to residual Cl vacancies, as previously discussed.[37] Surveying the ^{209}Bi MAS NMR (ESI,† Fig. S6) reveals a sizable chemical shift change of ~120 ppm between CABC (δ_{iso} = 4050 ppm, FWHM = 3.2 kHz) and CABSC (δ_{iso} = 3967 ppm, FWHM = 5.8 kHz). Furthermore, an increase in the spinning sideband manifold by *ca.* 50% (~320 *vs.* 460 kHz) is detected for the CABSC double perovskite phase. This experimental observation is consistent with an increasing perturbation of the bismuth electric field gradient (increase in quadrupole coupling) which would occur with an increase in atomic-level Sb/Bi disorder.[38]

Anion exchange with bromide: (i) the simpler case of substitutions in $Cs_2AgBiCl_6$

The Cl-to-Br exchange in CABSC double perovskites results in several events, including the anion exchange itself and the partial decomposition of the double perovskite into two different phases. To provide a more detailed description of these events, the Cl-to-Br substitutions in the Bi-only CABC double perovskite are first discussed in this section as the simpler case yielding single-phase products.

Interaction of CABC double perovskite with NaBr results in a change of coloration from pale yellow to deep orange, visually indicating the transformation of the original phase. A series of $Cs_2AgBi(Cl_{1-y}Br_y)_6$ compounds was obtained by adding different amounts of NaBr. The nominal Br fraction y was elevated up to 1.6 with respect to the stoichiometric amount needed to completely substitute Cl anions (that is y = 1.0).

The substitution of Cl is incomplete even at the over-stoichiometric amount of NaBr, at y = 1.4–1.6. The actual Br fraction in final products, y_a, determined by EDX, increases gradually with y reaching a plateau of y_a = 0.65–0.66 at y = 1.4–1.6 (Fig. 3a).

Powder XRD analysis of the anion-exchange products showed them to be single-phase cubic double perovskites similar to the original CABC with no new phases detected (ESI,† Fig. S7, left panel). From these data, the composition of

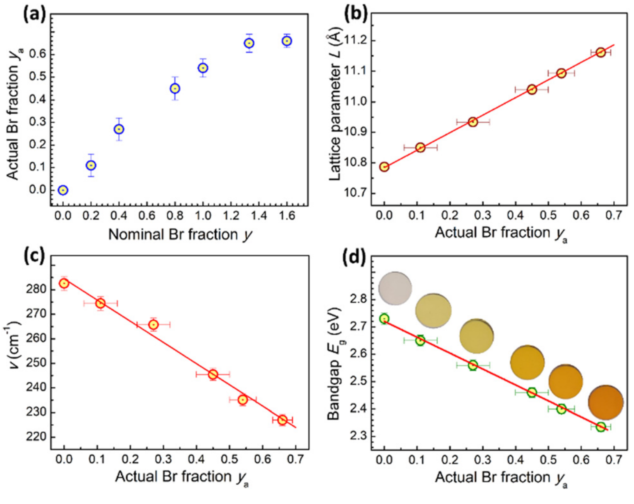

Fig. 3 (a) Actual molar Br fraction in CABCB perovskite y_a *versus* nominal Br fraction y during the substitution. (b)–(d) Lattice parameter L (scatter in (b)), frequency of the A_{1g} Raman band ν (scatter in (c)), and indirect bandgap E_g (scatter in (d)) of CABCB perovskites as functions of the actual Br fraction y_a; insert in (d) shows photographs of the substitution products for each particular point. Solid lines in (b)–(d) represent linear fitting of the experimental data with corresponding equations: $L = 10.785 + 0.574y_a$, $R^2 = 0.999$ (b), $\nu = 284.5 - 86.4y_a$, $R^2 = 0.985$ (c), and $E_g = 2.72 - 0.58y_a$, $R^2 = 0.995$ (d).

exchanged products with the maximal substitution depth can be inferred as $Cs_2AgBiCl_2Br_4$ (1/3 of original chloride remaining in the perovskite).

At lower amounts of Br the exchange results in the gradual substitution of Cl with the actual Br fraction y_a following the nominal Br fraction y in an almost linear manner (Fig. 3a). A closer look at the XRD reflections (ESI,† Fig. S7, right panel) shows several substituted forms to be present in equilibrium in each case. Nevertheless, the average lattice parameter shows a linear increase with y_a (Fig. 3b) indicating the formation of $Cs_2AgBi(Cl_{1-y}Br_y)_6$ solid solutions obeying Vegard's law.[6,7,19] The lattice expansion, in this case, originates from the larger size of the Br^- (192 pm) as compared to Cl^- (181 pm).[19]

SEM examination of the substitution products with different y (ESI,† Fig. S8) shows the same polycrystalline morphology observed earlier for the original Cl double perovskite.

Raman spectra of $Cs_2AgBi(Cl_{1-y}Br_y)_6$ compounds (ESI,† Fig. S9a) showed a gradual shift of the A_{1g} phonon frequency with a linear dependence on the actual Br fraction y_a (Fig. 3c), confirming the formation of solid-solution compounds.[6,7,19] This dependence encompasses a rather broad variation range, from 282 cm^{-1} for CABC to 223 cm^{-1} for the substituted compound with $y_a = 0.66$, allowing the composition of the Br–Cl mixed perovskites to be reliably identified from their Raman spectra.

The increase in the nominal Br fraction results in a gradual shift of the absorption band edge to lower energies, visualized by the change of coloration of the final products (see photograph in the insert in Fig. 3d). Similar to the original chloride perovskite, the absorption spectra of substitution products show extended linear edge sections when presented in the Tauc coordinates for both direct and indirect allowed electron transitions (ESI,† Fig. S9b and c), however, indirect bandgaps reflect more adequately the positions of absorption edge in original spectra. Moreover, the Br-pure and mixed Br/Cl Bi-based double perovskites revealed indirect bandgaps in theoretic modeling and experimental measurements.[6,7,19,22,23] In the present case, the indirect bandgap shows a linear dependence on the actual Br fraction y_a (Fig. 3d), indicating the formation of homogeneous solid solutions,[19] in agreement with the above-discussed XRD and Raman data as well as theoretical predictions.[23]

Anion exchange with bromide: (ii) the more complex case of $Cs_2AgBi_xSb_{1-x}Cl_6$

The interaction between Bi/Sb-mixed CABSC perovskites and NaBr results in a more complicated case with phase transformations of Sb-rich compounds, most probably due to the instability of double Ag–Sb bromide compounds.

In this series, freshly synthesized $Cs_2AgBi_xSb_{1-x}Cl_6$ perovskites with a varied Bi/Sb ratio x interacted with a fixed excess of NaBr ($y = 1.33$). EDX analysis of the final products showed the actual fraction of Bi, x_a, in all compounds to be close to the nominal one, x, set during the synthesis (Table 1). The x_a changes linearly with x (ESI,† Fig. S2b) and has a slope of approximate unity indicating a reliable control over the Bi/Sb ratio in the final anion-exchange products.

Table 1 Nominal (x) and actual (x_a) fraction of Bi, molar (Br + Cl)/(Bi + Sb) ratio, actual fraction of Br y_a, and molar Cs/(Bi + Sb) ratio for the products of Cl-to-Br substitution in $Cs_2AgBi_xSb_{1-x}Cl_6$ perovskites based on EDX analysis

x	x_a	(Br + Cl)/(Bi + Sb)	y_a	Cs/(Bi + Sb)
0	0	4.70	0.64	1.51
0.05	0.07 ± 0.04	4.45	0.65	1.53
0.10	0.12 ± 0.03	4.60	0.65	1.47
0.25	0.25 ± 0.02	5.55	0.66	1.68
0.50	0.47 ± 0.02	5.90	0.68	1.89
0.75	0.82 ± 0.02	6.00	0.67	1.96
0.90	0.94 ± 0.01	6.05	0.68	1.97
1.00	1.00	5.80	0.68	2.01

Similar to the above-discussed case of the Cl-to-Br exchange in CABC double perovskite, the anion exchange is incomplete even at the given excess of NaBr. The actual fraction of Br, y_a, varies around 0.66 (Table 1), indicating chloride is a third of the halide component of the final double perovskite.

The products synthesized in the range of x = 0–0.10 showed different ratios of total halide to total M^{III}, (Br + Cl)/(Bi + Sb) and Cs/(Bi + Sb) ratio, as compared to Sb-richer samples. For these compounds the ratios are around 4.5 and 1.5, respectively, suggesting a $Cs_3M_2X_9$ composition (Table 1) and confirmed by NMR, *vide infra*. The rest of the products with higher Bi contents shows (Br + Cl)/(Bi + Sb) of *ca.* 6 and Cs/(Bi + Sb) of *ca.* 2, indicating the formation of $Cs_2AgM^{III}X_6$ double perovskites. Taking into account the incomplete Br-to-Cl exchange with 1/3 Cl remaining in the structure, the chemical formulas for these cases can be presented as $Cs_3M^{III}_2Cl_3Br_6$ and $Cs_2AgM^{III}Cl_2Br_4$, respectively. The powder XRD results in general support these assessments and provide additional indications on the composition of the products of Cl-to-Br exchange. SEM examination of the exchange products showed them to be polycrystalline powders (ESI,† Fig. S4, middle column) with a relatively broad distribution of grain sizes in the range of a few µm. The morphology is roughly the same for the entire range of x. A fraction of thin-flake-like products was also observed for x = 0.10–0.25.

Rietveld analysis of the XRD patterns of Br-exchanged CABSC double perovskites revealed them to be a mixture of phases for all x's, except for the CABC compound (Fig. 4a and ESI,† Fig. S9). For the range of x = 0–0.10, the XRD patterns were satisfactorily fitted as mixtures of $Cs_3Bi_{2x}Sb_{2(1-x)}Cl_3Br_6$ (CBSCB) and AgBr (Fig. 4b and ESI,† Fig. S10). At higher contents of Bi ($x > 0.10$) the phase of double $Cs_2AgBi_xSb_{1-x}Cl_2Br_4$ (CABSCB) was detected. The relative content of this phase increased with x until the single phase was observed at x = 1.00.

The EDX analysis of Br-substituted samples revealed sodium admixtures in the entire range of x_a (ESI,† Table S2 and Fig. S11). At the same time, the ratio of Ag/(Bi + Sb) was found to be very close to 1 for all samples where the presence of double perovskite $Cs_2AgBi_xSb_{1-x}Cl_2Br_4$ was detected by XRD ($x_a > 0.12$, Fig. 4b). This observation indicates that no appreciable

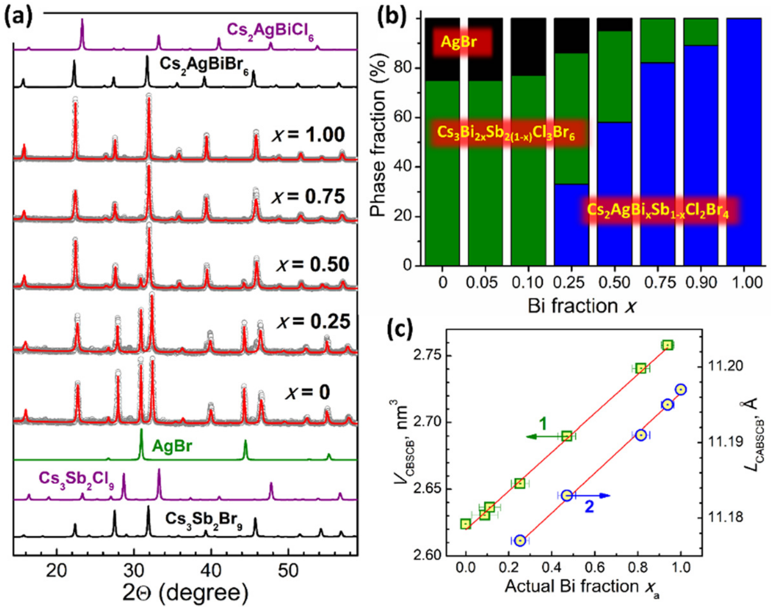

Fig. 4 (a) XRD profiles for the products of interaction between NaBr and $Cs_2AgBi_xSb_{1-x}Cl_6$ (CABSC) double perovskites with varied nominal Bi fraction x: gray scatter shows experimental data, solid red lines represent Rietveld refinement of the XRD patterns; in the lower and upper parts of the figure reference patterns are provided for $Cs_3Sb_2(Cl,Br)_9$, $Cs_2AgBi(Cl,Br)_6$, and AgBr. (b) Distribution of phases found by Rietveld refinement for the samples with different x. (c) Elementary cell volume of CBSCB (V_{CBSCB}, scatter 1) and lattice parameter of CABSCB (L_{CABSCB}, scatter 2) as functions of x_a; the solid red lines represent linear fits of the experimental data as $V_{CBSCB} = 2.620 + 0.146x_a$ (scatter 1) and $L_{CABSCB} = 11.170 + 0.026x_a$ (scatter 2). CBSCB is $Cs_3Bi_{2x}Sb_{2(1-x)}Cl_3Br_6$, and CABSCB is $Cs_2AgBi_xSb_{1-x}Cl_2Br_4$.

substitution of Ag^+ with Na^+ took place in the double perovskite during the anion exchange, the sodium admixture observed by EDX stemming most probably from residual NaBr/NaCl.

The elementary cell volume of $Cs_3Bi_{2x}Sb_{2(1-x)}Cl_3Br_6$ compounds changes linearly with x_a (Fig. 4c, scatter 1) indicating the formation of mixed Bi-Sb solid-solution series. Similarly, the lattice parameter of the double perovskite phase shows a linear increase with x_a, indicating the formation of the $Cs_2AgBi_xSb_{1-x}Cl_2Br_4$ solid solution.

The above XRD results (Fig. 4) indicate that mixed Bi/Sb double Br/Cl perovskites are unstable in the present conditions decomposing partially or completely with the formation of a $Cs_3Bi_{2x}Sb_{2(1-x)}Cl_3Br_6$ phase and silver being excluded in the form of AgBr. The instability of $Cs_2AgBi_xSb_{1-x}Cl_2Br_4$ double perovskites observed in the present conditions is in agreement with previous reports, indicating that antimony-substituted $Cs_2AgBiBr_6$ double perovskites can only accommodate *ca.* 40% of Sb^{III}, decomposing at higher Sb contents.[39,40]

Raman spectroscopy of the products of Cl-to-Br exchange supports the above assessments. The spectra registered for compounds with $x = 0$–0.25 have a distinctly different structure as compared with the Raman spectra of the products with higher Bi contents (Fig. 5a). The most prominent peaks in the Raman spectra of $Cs_3Sb_2Cl_3Br_6$ (the range of $x_a < 0.5$) can be observed at 208–209 cm^{-1} and 182–183 cm^{-1}, following A_{1g} and E_g frequencies reported for $Cs_3Sb_2Br_9$, 214 cm^{-1} and 184 cm^{-1}.[41] As the Bi content increases this peak shows a minor shift to a higher frequency (Fig. 5b), indicating that it comes from a phase with varied composition.

Raman spectra of the anion-exchanged products with $x_a > 0.5$ show the main peak at lower frequencies, gradually increasing from *ca.* 175 cm^{-1} for $x_a = 0.57$ to *ca.* 177 cm^{-1} for $x_a = 1.00$ (Fig. 5b), the latter value close to the reported A_{1g} frequencies of 177–180 cm^{-1} for $Cs_2AgBiBr_6$ double perovskite.[42,43] The gradual shift of the peak frequency with x is in line with the formation of solid-solution $Cs_2AgBi_xSb_{1-x}Cl_2Br_4$ compounds. The rather sharp change of the shape of Raman spectra observed at x_a of *ca.* 0.5 is also in line with the previous reports on the instability of $Cs_2AgBi_xSb_{1-x}Br_6$ double perovskites at $x_a < 0.6$.[39,40]

Similar to the above-discussed chloride double perovskites, the products of Cl-to-Br exchange show a deeper coloration for intermediate composition, as compared with the Sb-pure and Bi-pure products (photograph in the insert in Fig. 5c). The absorption edge of mixed compounds is shifted to lower energies reaching *ca.* 2.3 eV for the compound with $x_a = 0.47$ (Fig. 5c). The similarity with chloride compounds is continued by the fact that the absorption spectra of brominated products can be plotted in the Tauc coordinates of both direct and indirect allows transitions with linear sections of the absorption edge long enough for reliable determination of corresponding bandgaps (ESI,† Fig. S12), but the indirect E_g describing more realistically the position of the absorption band edge.

The bandgap of Bi-pure $Cs_2AgBiCl_2Br_4$ is higher than the values reported for Br-pure $Cs_2AgBiBr_6$, 1.9–2.19 eV,[14,22] additionally confirming the presence of chloride in the double chloro-bromide perovskite lattice. Similarly, the Sb-pure

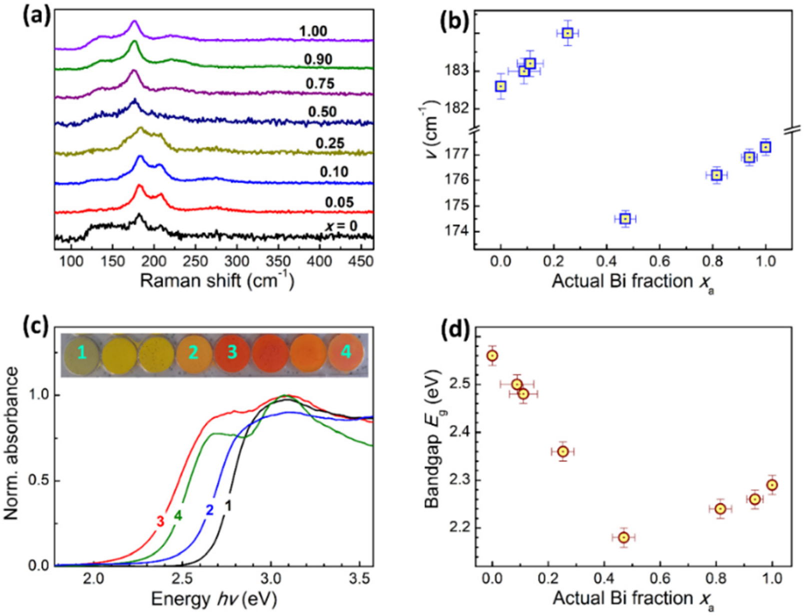

Fig. 5 (a) and (c) Raman (a) and absorption spectra (c) of the products of Cl-to-Br anion exchange in CABSC double perovskites with a varied nominal Bi fraction x; in (c) x = 0 (curve 1), 0.25 (2), 0.50 (3), and 1.00 (4), insert: photographs of anion-exchanged products with a varied x (numbers correspond to absorption spectra). (b) and (d) Frequency of the A_{1g} Raman peak v (b) and indirect bandgap E_g (d) of anion-exchanged products as a function of the actual Bi fraction x_a.

$Cs_3Sb_2Cl_3Br_6$ compound shows a somewhat higher indirect bandgap than reported for Br-pure $Cs_3Sb_2Br_9$, 2.43 eV.[41]

For mixed Bi/Sb products of anion exchange, the bandgap was found to be dependent on the Bi fraction, decreasing from E_g = 2.56 eV for Sb-pure product to 2.18 eV for x_a = 0.47 and increasing at higher actual fractions of Bi, reaching 2.29 eV for Bi-pure double perovskite (Fig. 5d). As with chloride perovskites, this trend indicates the band-bowing effect in $Cs_3Bi_{2x}Sb_{2(1-x)}Cl_3Br_6$ and $Cs_2AgBi_xSb_{1-x}Cl_2Br_4$. At that, the band-bowing in CBSCB perovskites is a major contributor to the descending section of $E_g(x_a)$ dependence (Fig. 5d) at $x_a < 0.5$, while the ascending "wing" of this dependence forms due to the band-bowing effect in CABSCB dominating at $x_a > 0.5$.

To ascertain atomic-level homogeneous mixing in the phases identified by XRD, complimentary ^{133}Cs MAS NMR spectroscopy measurements were performed for the identical series. The ^{133}Cs MAS NMR spectrum (Fig. 6a) of the Cl-to-Br exchange products of the $Cs_2AgSbCl_6$ phase with 0% Bi loading (x = 0) shows two resonances. The lower frequency resonance (δiso = 63 ppm) is consistent with the dominant form of $Cs_3Sb_2(Br,Cl)_9$ which has two distinct crystallographic Cs^+ sites as previously reported.[35,44–46] The higher frequency chemical shift at 83 ppm, is unresolved but should be in a 2 : 1 ratio with the lower frequency resonance. The small additional intensity is attributed to residual $Cs_2SbAg(Cl,Br)_6$ double perovskite phase ($Cs_2SbAgCl_6$, δ_{iso} = 82 ppm) reported by

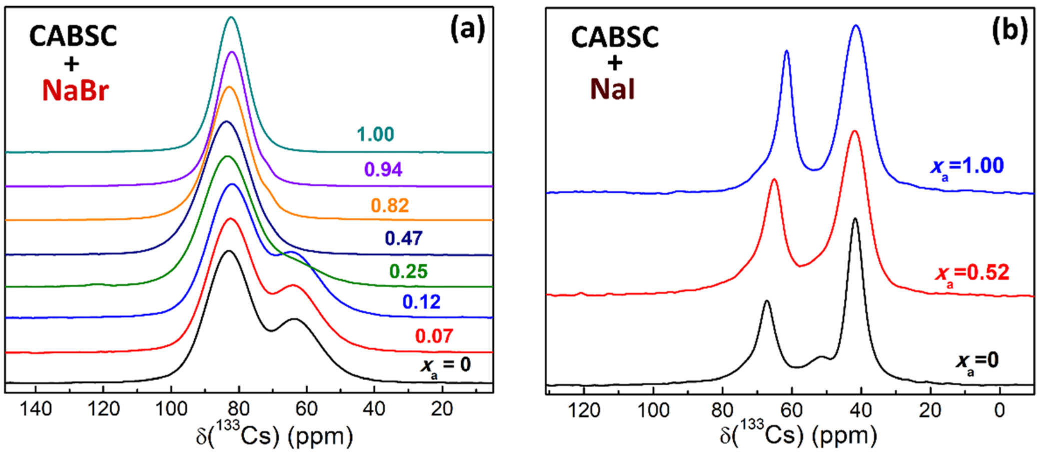

Fig. 6 ^{133}Cs MAS NMR spectra of the anion-exchange products of CABSC double perovskites with NaBr (a) and NaI (b).

Karmakar *et al.*[36] These results are consistent with previous reports for $Cs_3Sb_2Cl_9$ (δ_{iso} of 70 and 35 ppm),[36] $Cs_3Bi_2Br_9$ (δ_{iso} of 73 and 64 ppm),[46] and $Cs_3Bi_2I_9$ (δ_{iso} of ∼60 and ∼40 ppm).[34] A similar structure is observed in the ^{133}Cs MAS NMR spectra for the products with x_a = 0.07–0.12, where $Cs_3(Sb,Bi)_2(Br,Cl)_9$ phase dominates at low Bi concentrations. This finding supports the XRD observations and is consistent with atomic-level mixing of the M^{III} and X sites.

The trend changes at $x_a = 0.25$ where only a small residual shoulder can be observed at 63 ppm with a dominant CABSCB double perovskite phase (ESI,† Fig. S13a). At higher x_a values only a single resonance is observed at *ca.* 84 ppm (Fig. 6a, x_a = 0.47–1.00) assigned to the CABSCB phase with a single Cs site that appears to have a constant Cl/Br ratio. At the same time, the linewidth of this resonance shows a more regular dependence on the actual Bi fraction, increasing at small x_a, coming to saturation at x_a = 0.3–0.5, and then decreasing at higher Bi content (ESI,† Fig. S13b). This dependence can also indicate increased disorder in the mixed $Cs_3(Sb,Bi)_2(Br,Cl)_9$ and CABSCB double perovskite phases,[44–46] consistent with the optical band-bowing phenomena. The small shoulder ($x_a > 0.25$) is attributed to a minor secondary phase of $Cs_3(Sb,Bi)_2(Br,Cl)_9$.

Anion exchange with iodide

Interaction of CABSC double perovskites with NaI results in an instant transformation of chloride compounds into brightly colored reddish anion-exchange products. Inspection of the products with EDX analysis showed a close correspondence between the nominal Bi fraction x and the actual Bi fraction x_a (ESI,† Table S3 and Fig. S14). The $x_a(x)$ dependence is linear with a slope close to unity (ESI,† Fig. S2c), showing a perfect control over the Bi/Sb ratio in the final products. At the same time, the ratios of I/(Bi + Sb) and Cs(Bi + Sb) are close to 4.5 and 1.5 for the whole series range of x (ESI,† Table S3), respectively, both expected for the $Cs_3M_2^{III}I_9$ compounds.

In agreement with these expectations, the Rietveld analysis of XRD patterns of the NaI-treatment products revealed the presence of a single crystalline phase isostructural to $Cs_3Bi_2I_9$ (CBI)[47–49] with a varied Bi/Sb ratio (Fig. 7a).

The elementary cell volume increases linearly with an increase of the Bi fraction (Fig. 7b), indicating the formation of homogeneously alloyed solid-solution $Cs_3Bi_{2x}Sb_{2(1-x)}I_9$ compounds. No other phases were detected, with silver cations most probably excluded in the form of AgI and removed during the purification.

Similar to chloride and bromo-chloride compounds, SEM inspection revealed the I-exchanged products to be polycrystalline powders with no particular dependence of the morphology on the composition (ESI,† Fig. S4, right column). At high Bi contents (x = 0.75–1.00) formation of a minor fraction of hexagonal platelets was observed along with randomly aggregated perovskite microcrystals.

The ^{133}Cs MAS NMR spectra show two chemical shifts for the $Cs_3(Sb,Bi)I_9$ phase assigned to the two inequivalent Cs sites (Fig. 6b),[44,45] further supporting the conclusions made from the XRD data. One of the NMR peaks (Fig. 6b) shows a constant isotropic chemical shift of 42 ppm at different Bi fractions, while the second peak reveals a distinct compositional dependence, shifting from 67 ppm for $x_a = 0$ (*i.e.*, $Cs_3Sb_2I_9$, $\delta_{iso}(^{133}Cs)$

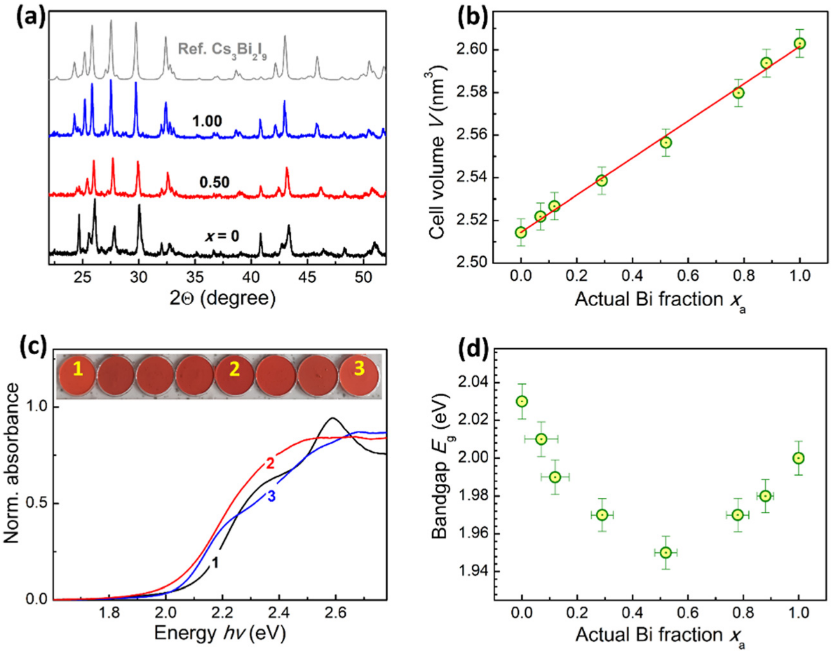

Fig. 7 (a) and (c) X-ray diffraction patterns (a) and absorption spectra (c) of CBSI perovskites with varied nominal Bi fraction x; in (c) x = 0 (curve 1), 0.50 (2), and 1.00 (3), insert: photographs of CBSI perovskites with a varied x (numbers correspond to absorption spectra). (b) and (d) Elementary cell volume V (b) and indirect bandgap (d) of CBSI perovskites as a function of the actual Bi fraction x_a; solid line in (b) represents the linear fit with expression $V = 2.514 + 0.087x_a$ (R^2 = 0.995).

of 42 and 67 ppm) to 66 ppm for $x_a = 0.52$ to 62 ppm for $x_a = 1.00$ (*i.e.*, $Cs_3Bi_2I_9$, $\delta_{iso}(^{133}Cs)$ of 42 and 62 ppm), the latter is consistent with ref. 35 and their reported chemical shift values for the $Cs_3Bi_2I_9$ phase.

The linewidth of this composition-dependent resonance increases from 6 ppm for $x_a = 0$ to 8 ppm for the mixed CBSI compound with $x_a = 0.52$ and then decreases again to 5 ppm for the bismuth-pure CBI compound. These observations are due to an increase in Sb/Bi random mixing,[44,45] and mirror the behavior observed in the CABSC double perovskites discussed above. The nature of a minor peak at *ca.* 52 ppm observed for the sample with $x_a = 0$ is an unidentified cesium-containing impurity. Further, this site mixing-induced disorder is also reflected in the ^{209}Bi NMR spectra for $Cs_3Bi_2I_9$ and $Cs_3(Sb,Bi)_2I_9$, with the broadening of the main Bi resonance for the mixed Sb/Bi compound (Fig. S15, ESI†).

By analogy with the original CABSC double perovskites the I-exchange products show deeper coloration for the intermediate composition, as compared to Sb- and Bi-only compounds (see photograph in the insert in Fig. 7c). The differences can also be observed in the position of the absorption edge, the mixed $Cs_3Bi_{2x}Sb_{2(1-x)}I_9$ compounds showing a shift of the edge position to lower energies (curve 2 in Fig. 7c) as compared to individual components (curves 1 and 3).

As in the cases of chloride and bromo-chlorides, both direct and indirect bandgaps can be estimated, the indirect E_g's showing a better match with the original absorption spectra (ESI,† Fig. S16). The indirect bandgap of $Cs_3Bi_{2x}Sb_{2(1-x)}I_9$ compounds decreases from $E_g = 2.03$ eV for Sb-pure compound down to 1.95 eV for $x_a = 0.52$, growing again at higher Bi content up to 2.00 eV for $Cs_3Bi_2I_9$ (Fig. 7d). Given the fact of the presence of a single phase, this bandgap variation can be attributed to the disorder-activated band-bowing effect, following the observations discussed above for ^{133}Cs MAS NMR spectra. This effect has not been reported before for Cs–Bi–I compounds, to the best of our knowledge, neither in experimental reports nor in theoretical predictions. It seems to be general for all studied mixed Bi/Sb materials, opening a new approach to bandgap design of metal halide perovskite and perovskite-inspired semiconductors by disorder-activated electronic effects. The family of $Cs_3Bi_2X_9$ (X = Cl, Br, I) compounds were reported to show a high degree of inherent disorder, even in the single-crystalline form,[47] allowing the even higher disorder to exist in mixed Bi/Sb analogs. A large room for bandgap variation can be expected from various disorder-activated effects in CBI perovskites, most probably reflected in a large scatter of reported bandgaps for this semiconductor, varying from 1.87 eV[48] to 2.24 eV.[49]

Conclusions

We report a mild synthesis of lead-free microcrystalline $Cs_2AgBi_xSb_{1-x}Cl_6$ (CABSC) double perovskites in the form of single-phase solid solutions with a varied Bi/Sb ratio. The CABSC perovskites revealed a compositional dependence of the bandgap, which decreases due to the Bi^{III} introduction into the $Cs_2AgSbCl_6$ matrix, reaches a minimum at $x = 0.26$, and then increases again for Bi-richer compositions. This band-bowing effect is attributed to a lattice disorder in CABSC perovskites based on disorder-related effects in ^{133}Cs MAS NMR spectra.

Interaction of CABSC perovskites with NaBr results in partial exchange of chloride with bromide as well as in the decomposition of the double Bi-Sb perovskite into a mixture of Bi/Sb phases, enriched with $Cs_3Bi_{2x}Sb_{2(1-x)}Cl_3Br_6$ at lower Bi contents and with $Cs_2AgBi_xSb_{1-x}Cl_2Br_4$ – at higher Bi contents. The Cl-to-Br anion-exchange products show a band-bowing behavior, with the minimal E_g reached at $x = 0.47$.

The Cl-to-I exchange in CABSC perovskites yields single-phase solid-solution $Cs_3Bi_{2x}Sb_{2(1-x)}I_9$ (CBSI) double salts with a varied Bi-to-Sb ratio. The CBSI compounds also reveal a band-bowing behavior with the minimal E_g observed at $x = 0.52$. Based on NMR results, this effect was also attributed to the lattice disorder caused by the Bi/Sb intermixing.

The present report highlights the possibility of a strong influence of lattice disorder and strain on the electronic properties of halide perovskite and perovskite-like compounds with two different M^{III} cations, in particular, by contributing to the optical band-bowing behavior. A deeper understanding and mastering of such band-bowing effects can lead to new PV materials with reduced band gaps.

Author contributions

O. Stroyuk: conceptualization (lead), investigation (equal), writing – original draft preparation (lead); O. Raievska: investigation (lead), methodology (lead); A. Barabash: investigation (equal), writing – review & editing (equal); R. W. Hooper: investigation (equal), writing – review & editing (equal); V. K. Michaelis: conceptualization (equal), writing – review & editing (equal), project administration (lead), funding acquisition (lead); J. Hauch: conceptualization (equal), project administration (lead), writing – review & editing (equal); C. J. Brabec: conceptualization (equal), funding acquisition (lead), writing – review & editing (equal).

Conflicts of interest

There are no conflicts to declare.

Acknowledgements

The authors gratefully acknowledge the financial support of The German Federal Ministry for Economic Affairs and Climate Action (project Pero4PV, FKZ: 03EE1092A) and The Bavarian State Government (project ''ELF-PV-Design and development of solution-processed functional materials for the next generations of PV technologies'', No. 44-6521a/20/4). VKM acknowledges research support from the Natural Sciences and Engineering Research Council of Canada Discovery Grant (RGPIN-2021-02540) and Create (ATUMS), Alberta Innovates

Strategic Project, and Canada Research Chairs (CRC-2020-00352) programs. The Canada Foundation for Innovation (CFI), the Government of Alberta, and the University of Alberta are acknowledged for supporting the Chemistry Centre for Magnetic Resonance (C^{2}MR), a core characterization facility within the Faculty of Science, CNAS.

References

1 Y. Cui, L. Yang, X. Wu, J. Deng, X. Zhang and J. Zhang, *J. Mater. Chem. C*, 2022, **10**, 16629.
2 H. Yin, Y. Xian, Y. Zhang, W. Li and J. Fan, *Sol. RRL*, 2019, 1900148.
3 W. Ning and F. Gao, *Adv. Mater.*, 2019, 1900326.
4 Y. Li, Z. Shi, W. Liang, J. Ma, X. Chen, D. Wu, Y. Tian, X. Li, C. Shan and X. Fang, *Mater. Horiz.*, 2021, **8**, 1367.
5 X. Li, X. Gao, X. Zhang, X. Shen, M. Lu, J. Wu, Z. Shi, V. L. Colvin, J. Hu, X. Bai, W. W. Yu and Y. Zhang, *Adv. Sci.*, 2021, **8**, 2003334.
6 H. Lei, D. Hardy and F. Gao, *Adv. Funct. Mater.*, 2021, **31**, 2105898.
7 X. Yang, W. Wang, R. Ran, W. Zhou and Z. Shao, *Energy Fuels*, 2020, **34**, 10513.
8 S. Attique, N. Ali, S. Ali, R. Khatoon, N. Li, A. Khesro, S. Rauf, S. Yang and H. Wu, *Adv. Sci.*, 2020, **7**, 1903143.
9 Y. Peng, T. N. Huq, J. Mei, L. Portilla, R. A. Jagt, L. G. Occhipinti, J. L. MacManus-Driscoll, R. L. Z. Hoye and V. Pecunia, *Adv. Energy Mater.*, 2021, **11**, 2002761.
10 N. Glück and T. Bein, *Energy Environ. Sci.*, 2020, **13**, 4691.
11 S. E. Creutz, E. N. Crites, M. C. De Siena and D. R. Gamelin, *Nano Lett.*, 2018, **18**, 1118.
12 O. Stroyuk, O. Raievska, A. Barabash, M. Batentschuk, A. Osvet, S. Fiedler, U. Resch-Genger, J. Hauch and C. J. Brabec, *J. Mater. Chem. C*, 2022, **10**, 9938.
13 O. Stroyuk, O. Raievska, A. Barabash, C. Kupfer, A. Osvet, V. Dzhagan, D. R. T. Zahn, J. Hauch and C. J. Brabec, *Mater. Adv.*, 2022, **3**, 7894.
14 E. T. McClure, M. R. Ball, W. Windl and P. M. Woodward, *Chem. Mater.*, 2016, **28**, 1348.
15 J. Zhou, X. Rong, M. S. Molokeev, X. Zhang and Z. Xia, *J. Mater. Chem. A*, 2018, **6**, 2346.
16 J. E. F. S. Rodrigues, C. A. Escanhoela, Jr., B. Fragoso, G. Sombrio, M. M. Ferrer, C. Álvarez-Galván, M. T. Fernández-Díaz, J. A. Souza, F. F. Ferreira, C. Pecharromán and J. A. Alonso, *Ind. Eng. Chem. Res.*, 2021, **60**, 18918.
17 A. Singh, R. Chaurasiya, A. Bheemaraju, J. S. Chen and S. Satapathi, *ACS Appl. Energy Mater.*, 2022, **5**, 3926.
18 B. Yang, F. Hong, J. Chen, Y. Tang, L. Yang, Y. Sang, X. Xia, J. Guo, H. He, S. Yang, W. Deng and K. Han, *Angew. Chem., Int. Ed.*, 2019, **58**, 1.
19 A. C. Dakshinamurthy, M. Gupta, B. R. Kumar Nanda and C. Sudakar, *J. Phys. Chem. C*, 2023, **127**, 1588.
20 D. Manna, J. Kangsabanik, T. K. Das, D. Das, A. Alam and A. Yella, *J. Phys. Chem. Lett.*, 2020, **11**, 2113.
21 A. S. Kshirsagar and A. Nag, *J. Chem. Phys.*, 2019, **151**, 161101.
22 M. R. Filip, S. Hillman, A. A. Haghighirad, H. J. Snaith and F. Giustino, *J. Phys. Chem. Lett.*, 2016, **7**, 2579.
23 J. Su, T. Mou, J. Wen and B. Wang, *J. Phys. Chem. C*, 2020, **124**, 5371.
24 D. Mourad and G. Czycholl, *Eur. Phys. J. B*, 2012, **85**, 153.
25 A. Zunger and J. E. Jaffe, *Phys. Rev. Lett.*, 1983, **51**, 662.
26 J. Im, C. C. Stoumpos, H. Jin, A. J. Freeman and M. G. Kanatzidis, *J. Phys. Chem. Lett.*, 2015, **6**, 3503.
27 G. E. Eperon, T. Leijtens, K. A. Bush, R. Prasanna, T. Green, J. T. W. Wang, D. P. McMeekin, G. Volonakis, R. L. Milot, R. May, A. Palmstrom, D. J. Slotcavage, R. A. Belisle, J. B. Patel, E. S. Parrott, R. J. Sutton, W. Ma, F. Moghadam, B. Conings, A. Babayigit, H. G. Boyen, S. Bent, F. Giustino, L. M. Herz, M. B. Johnston, M. D. McGehee and H. J. Snaith, *Science*, 2016, **354**, 861.
28 A. Goyal, S. McKechnie, D. Pashov, W. Tumas, M. Van Schilfgaarde and V. Stevanovic, *Chem. Mater.*, 2018, **30**, 3920.
29 S. Dai, X. Gan, K. Li, Q. Huang, L. Guo and H. Liu, *Phys. Chem. Chem. Phys.*, 2023, **25**, 30993.
30 G. Giovilli, B. Albini, V. Grisci, S. Bonomi, M. Moroni, E. Mosconi, W. Kaiser, F. De Angelis, P. Galinetto and L. Malavasi, *J. Mater. Chem. C*, 2023, **11**, 10282.
31 Z. Li, S. R. Kavanagh, M. Napari, R. G. Palgrave, M. Abdi-Jalebi, Z. Andaji-Garmaroudi, D. W. Davies, M. Laitinen, J. Julin, M. A. Isaacs, R. H. Friend, D. O. Scanlon, A. Walsh and R. L. Z. Hoye, *J. Mater. Chem. A*, 2020, **8**, 21780.
32 H. Chen, S. Ming, M. Li, B. Wang and J. Su, *J. Phys. Chem. C*, 2021, **125**, 11271.
33 F. Ji, J. Klarbring, F. Wang, W. Ning, L. Wang, C. Yin, J. S. Mendoza Figueroa, C. K. Christensen, M. Etter, T. Ederth, L. Sun, S. I. Simak, I. A. Abrikosov and F. Gao, *Angew. Chem.*, 2020, **132**, 15303.
34 J. Yang, P. Zhang and S. H. Wei, *J. Phys. Chem. Lett.*, 2018, **9**, 31.
35 D. J. Kubicki, M. Saski, S. MacPherson, K. Galkowski, J. Lewinski, D. Prochowicz, J. J. Titman and S. D. Stranks, *Chem. Mater.*, 2020, **32**, 8129.
36 A. Karmakar, M. S. Dodd, S. Agnihotri, E. Ravera and V. K. Michaelis, *Chem. Mater.*, 2018, **30**, 8280.
37 A. Karmakar, G. M. Bernard, A. Meldrum, A. O. Oliynyk and V. K. Michaelis, *J. Am. Chem. Soc.*, 2020, **142**, 10780.
38 A. Karmakar, G. M. Bernard, A. Pominov, T. Tabassum, R. Chaklashiya, S. Han, S. K. Jain and V. K. Michaelis, *J. Am. Chem. Soc.*, 2023, **145**, 4485.
39 E. M. Hutter, M. C. Gelvez-Rueda, D. Bartesaghi, F. C. Grozema and T. J. Savenje, *ACS Omega*, 2018, **3**, 11655.
40 K. Du, W. Meng, X. Wang, Y. Yan and D. B. Mitzi, *Angew. Chem., Int. Ed.*, 2017, **56**, 8158.
41 A. Pradhan, M. K. Jena and S. L. Samal, *ACS Appl. Energy Mater.*, 2022, **5**, 6952.
42 R. Kentsch, M. Scholz, J. Horn, D. Schlettwein, K. Oum and T. Lenzer, *J. Phys. Chem. C*, 2018, **122**, 25940.
43 P. Pistor, M. Meyns, M. Guc, H. C. Wang, M. A. L. Marques, X. Alcobe, A. Cabot and V. Izquierdo-Roca, *Scr. Mater.*, 2020, **184**, 24.
44 Yu. N. Ivanov, A. A. Sukhovskii, V. V. Lisin and I. P. Aleskandrova, *Inorg. Mater.*, 2001, **37**, 623.

45 C. J. Krajewska, S. R. Kavanagh, L. Zhang, D. J. Kubicki, K. Dey, K. Gałkowski, C. P. Grey, S. D. Stranks, A. Walsh, D. O. Scanlon and R. G. Palgrave, *Chem. Sci.*, 2021, **12**, 14686.

46 A. Elattar, L. Kobera, J. Kangsabanik, H. Suzuki, S. Abbrent, T. Nishikawa, K. S. Thygesen, J. Brus and Y. Hayashi, *J. Mater. Chem. C*, 2022, **10**, 12863.

47 N. K. Tailor and S. Satapathi, *ACS Appl. Energy Mater.*, 2020, **3**, 11732.

48 A. Nila, M. Baibarac, A. Matea, R. Mitran and I. Baltog, *Phys. Status Solidi B*, 2017, **254**, 1552805.

49 S. K. Shil, F. Wang, Z. Lai, Y. Meng, Y. Wang, D. Zhao, M. K. Hossain, K. O. Egbo, Y. Wang, K. M. Yu and J. C. Ho, *Nano Res.*, 2021, **14**, 4116.